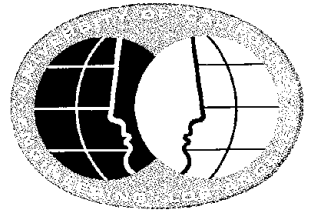


USF-RA-E-75-220

**UCLA-ENG-7497  
DECEMBER 1974**

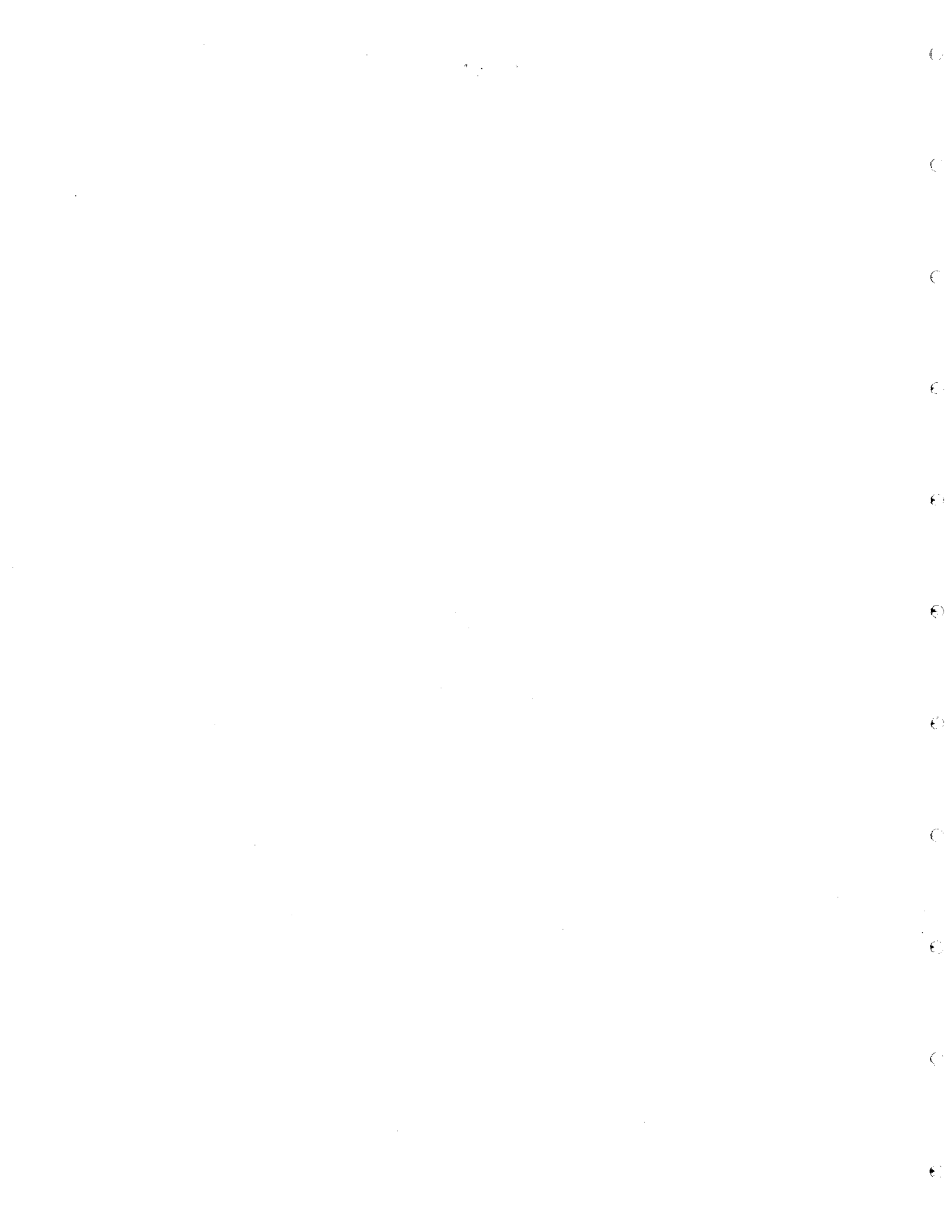


**Report to the  
National Science Foundation  
Project GI 38521**

# **SEISMIC PERMANENT DEFORMATIONS IN EARTH DAMS**

**Principal Investigator: Kenneth L. Lee**

REPRODUCED BY  
**NATIONAL TECHNICAL  
INFORMATION SERVICE**  
U. S. DEPARTMENT OF COMMERCE  
SPRINGFIELD, VA. 22161



<b>BIBLIOGRAPHIC DATA SHEET</b>	1. Report No. NSF-RA-E-75-220	2.	3. Recipient's Accession No. 3843
	4. Title and Subtitle Seismic Permanent Deformations in Earth Dams		5. Report Date December 1974
7. Author(s) K.L.Lee		8. Performing Organization Repr. No. UCLA-ENG-7497	
9. Performing Organization Name and Address University of California School of Engineering and Applied Science Mechanics and Structures Department Los Angeles, California 90024		10. Project/Task/Work Unit No.	
		11. Contract/Grant No. GI38521	
12. Sponsoring Organization Name and Address Research Applied to National Needs (RANN) National Science Foundation Washington, D.C. 20550		13. Type of Report & Period Covered	
		14.	
15. Supplementary Notes			
16. Abstracts This report considers the problem of estimating the permanent deformations that are likely to occur as a result of an earthquake. The basic concept involves the assumption that seismic induced deformations are due to a softening of the soil by seismic shaking so that following the earthquake the embankment will settle or deform to a new condition compatible with the new "softened" stiffness of the soil. A method for estimating this softening effect from the results of cyclic laboratory tests is described as well as a method of formulating the analysis into a pseudo static type of finite element program. The relevance of this new type of analysis to actual problems is illustrated by analyzing 5 different dams which have been damaged by previous earthquakes. A fair agreement was found between the predicted and the observed deformations.			
17. Key Words and Document Analysis. 17a. Descriptors			
Earthquakes		Distortion	
Dams		Deformation methods	
Earth dams		Structural analysis	
Embankments		Seismology	
Deformation		Stresses	
Damage		Stress analysis	
17b. Identifiers/Open-Ended Terms			
Seismic permanent deformations			
17c. COSATI Field/Group			
18. Availability Statement NTIS		19. Security Class (This Report) UNCLASSIFIED	
		20. Security Class (This Page) UNCLASSIFIED	22. Price Aφ3 - Aφ1



Seismic Permanent Deformations In Earth Dams

by

Kenneth L. Lee


Report to the  
National Science Foundation  
Project GI 38521

Principal Investigator: Kenneth L. Lee

Mechanics and Structures Department  
School of Engineering and Applied Science  
University of California  
Los Angeles, California

December 1974

Any opinions, findings, conclusions  
or recommendations expressed in this  
publication are those of the author(s)  
and do not necessarily reflect the views  
of the National Science Foundation.





## Synopsis

Analytical methods of seismic stability analysis of earth embankments currently in use (1974) are based on a limiting equilibrium concept that if the calculated seismic stresses are less than the cyclic strength of the soil, the dam is safe. If the calculated seismic stress are greater than the cyclic strength then the embankment is unsafe. There is currently no method of calculating intermediate conditions of some non-failure deformations. A strain potential can be estimated, based on the predicted performance of a sample of soil in a laboratory cyclic loading test simulating the field seismic loading, but this strain potential is only related to the field performance of the dam through qualitative and empirical estimates.

This report considers the problem of estimating the permanent deformations that are likely to occur as a result of an earthquake. The basic concept involves the assumption that seismic induced deformations are due to a softening of the soil by seismic shaking so that following the earthquake the embankment will settle or deform to a new condition compatible with the new "softened" stiffness of the soil. A method for estimating this softening effect from the results of cyclic laboratory tests is described as well as a method of formulating the analysis into a pseudo static type of finite element program. The relevance of this new type of analysis to actual problems is illustrated by analyzing 5 different dams which have been damaged by previous earthquakes. A fair agreement was found between the predicted and the observed deformations.





# SEISMIC PERMANENT DEFORMATIONS IN EARTH DAMS

BY

KENNETH L. LEE<sup>1</sup>

## INTRODUCTION

Most currently used methods of seismic stability analysis for earth dams are based on a limiting equilibrium concept. A general description of this method attributed to Hardy Cross is that "a structure breaks if it does not hold together". The results of limiting equilibrium calculations are conveniently expressed in terms of a single number such as a safety factor, which is then interpreted to indicate whether the dam is or is not stable under the specified loading conditions.

The oldest limiting equilibrium method of seismic slope stability analysis is the so called pseudo static method (18,26). This is a slip surface method using static soil strengths along with one additional force to account for the effects of the earthquake. The evaluation of this additional seismic force is entirely empirical and therefore rather arbitrary. As expressed by Terzaghi almost 25 years ago, this method is not necessarily very reliable (27).

An improvement in the slip surface method of seismic stability analysis, suggested by Seed (15) in 1966, involved determining soil strengths from cyclic loading tests, and calculating the seismic coefficient (17) by seismic response analysis using a method proposed by Ambraseys (1). Lee and Walters have used this method, with some success, in studying the behavior of the Dry Canyon Dam during the 1952 Kern County earthquake (7).

A method for calculating the permanent deformations in slopes resulting from seismic loading was suggested by Newmark (12). This was based on the pseudo-static yield method, except that the seismic coefficient was allowed to vary with time throughout the duration of the earthquake. A pseudo-static yield acceleration was calculated which would just cause the slope to be unstable, and this was compared with the actual acceleration time history. By double integration, a progressive time history of slope deformation may be calculated. This method has been used successfully by Goodman and Seed (4) to analyze the results from model shaking table tests of dry sand slopes. It is difficult to apply the method to saturated soils, because of uncertainty in evaluating the actual

---

<sup>1</sup>Associate Professor, School of Engineering and Applied Science, University of California at Los Angeles.

time history of pore pressure, effective stress and soil strength during cyclic loading (19). Furthermore, the yield acceleration must be evaluated in terms of an overall equilibrium failure criteria, and therefore involves much the same objections as the other limiting equilibrium methods.

A major advance in seismic slope stability analysis has been made by using the finite element method to calculate both the static and the earthquake induced stresses at all locations throughout the embankment. Comparison of the seismic stresses with the soil strengths determined from cyclic loading tests on samples consolidated to appropriate static stress conditions leads to an assessment of the stability of each finite element. The ultimate performance of the whole dam is then postulated, based on the distribution of the calculated stability throughout the dam. This method has been successfully used to analyze the failures of the Sheffield Dam during the Santa Barbara Earthquake of 1925 (20) and the performance of the Upper and Lower San Fernando Dams during the San Fernando Earthquake of 1971 (22).

For many cases, the calculated seismic stress will be sufficiently greater or smaller than the measured cyclic strengths to indicate clearly whether or not a slope will be stable. Difficulties in interpretation arise when the calculated and measured strengths have similar values at a few elements, or where weak elements are surrounded by much stronger soil. As an extreme illustrative example, a tank of saturated sand on a shaking table may completely liquefy, but if the walls of the container do not fail, the sand will not flow; and the permanent shear deformations will be zero. Thus an evaluation of the overall performance of an embankment requires an examination of all elements together.

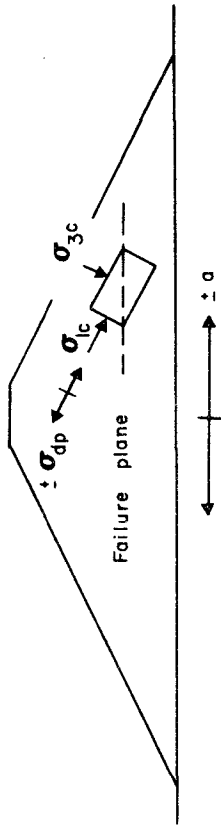
Therefore, to assist in evaluating the overall seismic stability of an earth dam, a method is proposed for calculating the overall permanent deformations resulting from the effect of a given earthquake motion. Because the proposed method involves many of the techniques already in use, it will be introduced by a brief background summary of the existing method of seismic stability analysis using finite elements.

#### FINITE ELEMENT METHOD OF SEISMIC STABILITY ANALYSIS

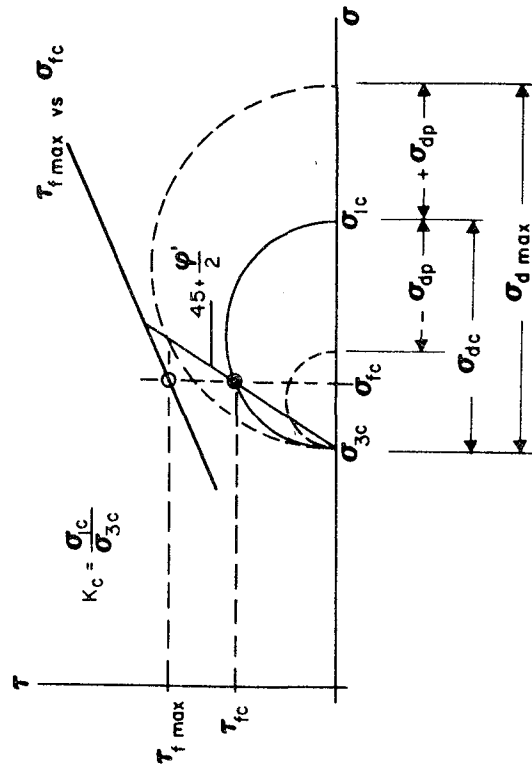
Several key features of the finite element approach to the seismic stability analysis of embankments are shown on Fig. 1. The pre-earthquake static stress  $\sigma_{fc}$  and  $\tau_{fc}$ , at each element are readily determined by a static loading finite element program, including gravity and seepage effects.

It is noted that the stress components of interest are those which act on horizontal planes. The subscript c refers to stresses after consolidation, and the subscript f suggests that these will be on a potential failure plane during the earthquake. The earthquake induced accelerations of  $\pm a$ , at the base of the dam, produce the cyclic shear stresses  $\pm \tau_p$  on the horizontal planes as evaluated by an appropriate computer program (5).

The soil strength  $\tau_{f \max}$ , to be used in the seismic stability analysis would logically be determined by cyclic loading tests on

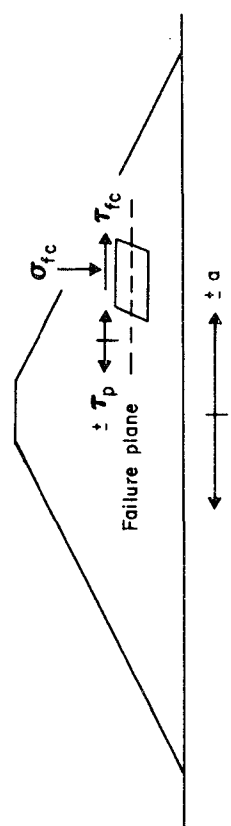


(a) Field Element

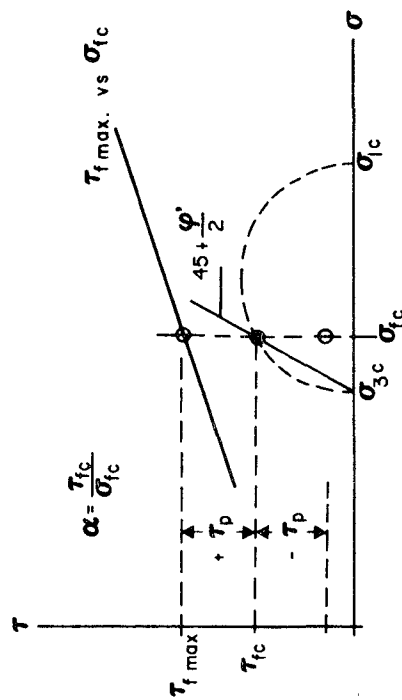


(b) Mohr Diagram

FIG. 2 CYCLIC LOADING SIMULATION BY TRIAXIAL TEST.



(a) Field Element



(b) Mohr Diagram

FIG. 1 CYCLIC LOADING SIMULATION BY SIMPLE SHEAR TEST.

simple shear samples which resemble the typical element shown in Fig. 1a. However, since triaxial test equipment is currently more readily available than simple shear equipment, the present practice uses triaxial tests almost exclusively. Correspondence between triaxial and simple shear or field stresses is shown on Figs. 1 and 2.

The triaxial test specimens are consolidated to the appropriate normal and shear stresses corresponding to elements in the field, and then subjected to cyclic stresses until they fail. Failure is usually defined in terms of a specified axial strain. Sufficient tests are required to cover the range of stress conditions developed throughout the dam and the strength of the soil at each element is obtained by interpolation from the test data. In this regard, it is convenient to perform the tests, express the results, and tabulate the pre-earthquake field stresses in terms of normal consolidation stress on the failure plane  $\sigma_{fc}$ , and anisotropic consolidation stress ratio  $\alpha = \tau_{fc}/\sigma_{fc}$  or  $K_c = \sigma_{1c}/\sigma_{3c}$  as shown in Figs. 1 and 2.

Unfortunately, the cyclic loading triaxial test reproduces only some of the essential field conditions. Corrections are required to compensate for the inherent differences. For the special case of  $\alpha = 0$  ( $K_c = 1.0$  in triaxial tests), the correct field cyclic shear strength  $\tau_p$  may be determined from the laboratory pulsating strength  $\sigma_{dp}$  using a correction factor  $C_r$  in the following equation (21):

$$\left(\frac{\tau_p}{\sigma_{fc}}\right)_{\text{field}} = C_r \left(\frac{\sigma_{dp}}{2\sigma_{3c}}\right)_{\text{lab}} \quad (1)$$

Values for  $C_r$  ranges from about 0.55 for loose sand to 0.8 for dense sand. For anisotropic consolidation corresponding to  $K_c \geq 1.5$ ,  $C_r = 1.0$  (20). Linear interpolation is used in the range  $1.0 < K_c < 1.5$ . Because laboratory tests are performed using uniform cyclic loads, the actual erratic field stress time-history must be converted to an equivalent average shear stress  $\tau_{av}$  corresponding to a number of equivalent uniform cycles  $N_{eq}$  (8). Studies have shown that for any constant value of  $N_{eq}$ , an almost constant ratio exists between the equivalent average and the maximum seismic shear stress  $\tau_m$  at all locations in the embankment:

$$R = \frac{\tau_{av}}{\tau_m} \quad (2)$$

Thus only  $\tau_m$  need be printed out for each element from the seismic stress analysis. The entire time history of calculated cyclic shear stress is saved for only a few elements, from which representative values of  $R$  and  $N_{eq}$  are calculated. The value of  $\tau_{av}$  is then computed from Eq. 2 and used in the subsequent stability calculations.

Having thus determined the pulsating loading strength  $\tau_p$ , and the induced seismic stress  $\tau_{av}$ , the next logical step is to compare these values. A convenient comparison is in terms of a factor of specified performance for each element:

$$FSP = \frac{\tau_p}{\tau_{av}} \quad (3)$$

This is similar to a conventional safety factor, except that it refers only to each element separately rather than to the entire structure as a whole.

Since the pulsating loading strength is defined rather arbitrarily by the amount of axial strain developed in a laboratory sample under  $N_{eq}$  cycles, it follows that different values of FSP can be obtained by selecting different strength criteria. For soils

such as loose saturated sands, which strain very little during the first few cycles, but then loose considerable strength, or liquefy with additional cyclic loading, the calculated values of FSP are almost independent of the specified definition for failure in laboratory specimens. For dense sands and compacted clays, which never suddenly collapse but which deform progressively with each successive cycle, the FSP can be quite sensitive to the selected failure criteria.

An alternative method of expressing the final result of a seismic stability analysis is in terms of the amount of strain that a sample of soil would undergo in a laboratory test if subjected to the equivalent pulsating stresses of an earthquake (22). It is emphasized that this strain potential refers only to strains in individual laboratory samples, and not to the strains which would develop at different elements in the field.

For design purposes, values of FSP or strain potential are calculated for each finite element, and may be displayed numerically or by contours on the cross section of the dam. Engineering judgment is then required to interpret whether or not the entire embankment will perform satisfactorily under the design earthquake. Clearly, if almost all elements show satisfactory performance, the entire dam will be assumed stable and vice versa. Difficulties in interpretations for the whole dam arise when more than a few, but less than the majority of elements show individual unsatisfactory performance.

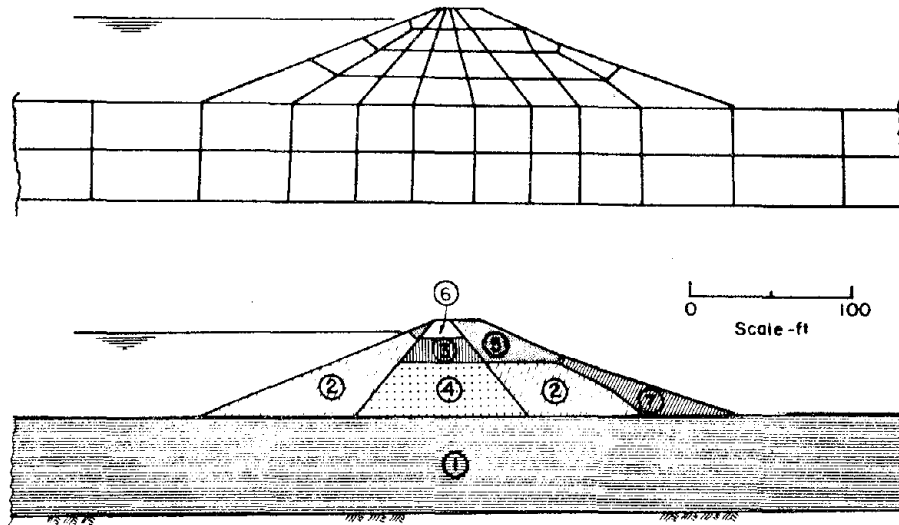
#### ILLUSTRATIVE EXAMPLE - DRY CANYON DAM

Confidence in any method of analysis comes from comparing calculations with actual case history observations. The above method has been successfully used to analyze the unsatisfactory performance of the Sheffield dam (20) and the two San Fernando dams (22). As a further illustration of the method, and as an introduction to the permanent deformation method to be described hereafter, some results from calculations for the Dry Canyon dam are presented herein.

A study of the behavior of this dam to the 1952 Kern County earthquake, based on the slip circle type of analysis proposed by Seed (15) has been previously described (7) so only essential details are repeated here. The earthquake registered a Richter magnitude of 7.7. The dam was about 46 miles from both the epicenter and the causative fault. It suffered some cracks along the crest, as well as permanent vertical settlement and upstream movement of about 0.3 feet. Strong motion accelerograms were obtained at various distances from the epicenter, the closest being at Taft, about 25 miles distant, which recorded accelerations of 0.178g horizontal and 0.116g vertical. All of the recorded peak accelerations fall within the band proposed by Schnabel and Seed (14) for M 7.6 earthquakes. At the epicenter distance of the dam, this band indicates possible peak accelerations ranging from 0.07g to 0.16g.

The Dry Canyon Dam is an old combined hydraulic fill and wagon rolled embankment built around 1912. It is 63 feet high and is founded on about 60 feet of granular alluvium. A view of the maximum cross section showing the various interior zones and the finite element representation is presented in Fig. 3. The soil in

the different zones was similar in texture, being coarse to fine silty sands. From the seismic stability point of view, the principal differences were in the relative densities.



Zone	Below WT	Above WT	Dr - %
Foundation	1	—	77
Shell	2	5	62
Wagon Rolled Core	3	6	68
Hydraulic Fill Core	4	—	47
Stabilizing Berm	—	7	80

FIG. 3 FINITE ELEMENT SIMULATION OF DRY CANYON DAM.

Cyclic loading triaxial tests were performed on reconstituted samples of the soil compacted to 50 percent relative density. One record of a typical cyclic loading test results is shown in Fig. 4. The results of 5 typical tests on samples all consolidated to the same static effective stress conditions are shown on Fig. 5. These data illustrate how the strength is obtained for any specified axial strain criteria. For the example calculations described herein, the strength was determined by  $\epsilon_1 = 5\%$  (single amplitude).

The cyclic loading strength at each finite element in the dam was obtained by interpolation among several sets of test data, such as shown on Fig. 5b, for the appropriate density and static confining pressure at the element.

Several finite element seismic response analyses were performed using both the horizontal and the vertical acceleration components simultaneously, each analyses used the Taft accelerograms, but with all accelerations scaled to give the desired peak horizontal acceleration. The analyses indicated that the actual erratic stress history could be represented by  $N_{eq} = 10$  uniform cycles and  $R = 0.72$ . Thus, for each set of test data such as illustrated in Fig. 5b, the cyclic loading strength was obtained for  $\epsilon_1 = 5\%$  and  $N = 10$  cycles. These laboratory strengths were then converted to field conditions

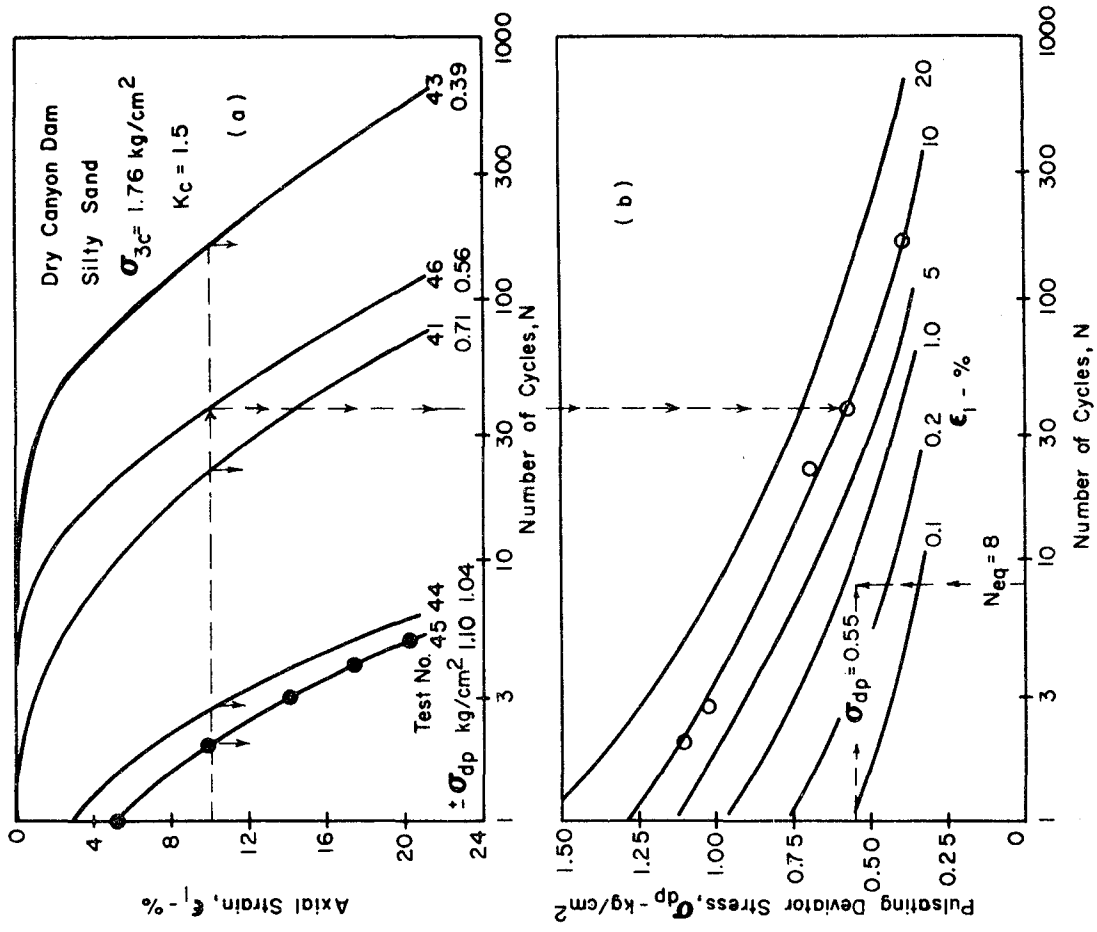


FIG. 5 DATA FROM TYPICAL PULSATING LOAD TESTS.

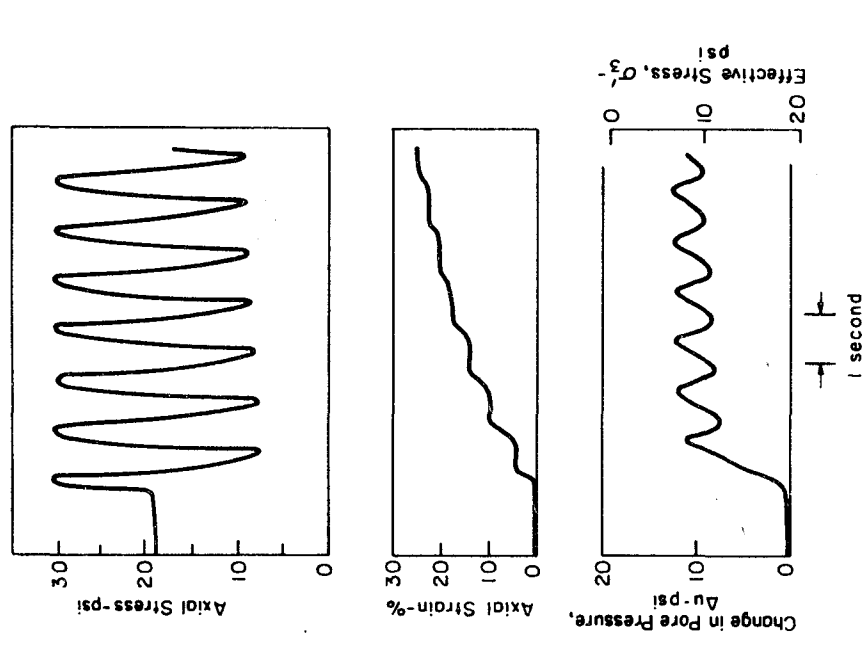
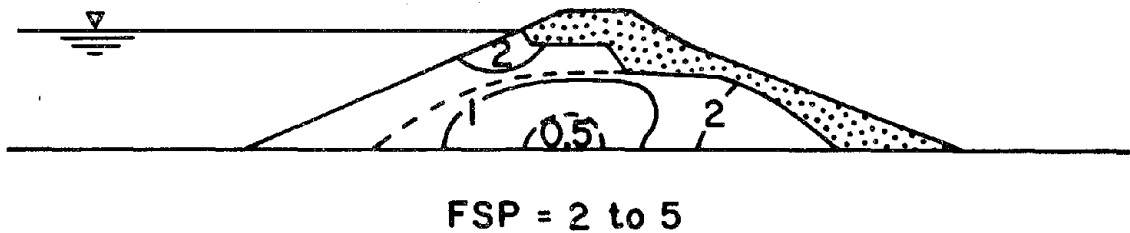


Fig. 4 TYPICAL PULSATING LOAD TESTING RECORD.

as described in the previous section, and values of FSP were calculated for each element by Eq. 3.

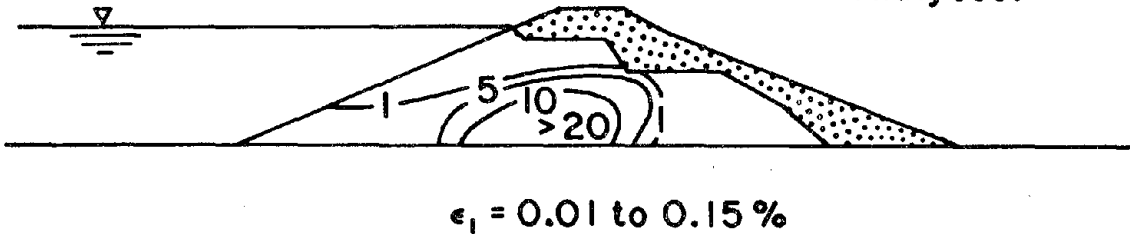
The first analysis was made for an assumed maximum peak horizontal acceleration of 0.1g corresponding to the median of the range of probable accelerations at the site. The results of the analyses are summarized in Fig. 6a which shows contour lines drawn through elements with similar values of FSP. The analysis indicates that the foundation and the outer shell of the dam had values of FSP greater than 1.0, indicating satisfactory performance, but the calculated performance of a large interior was unsatisfactory.

Using the same data, calculations were also made of the strain potential for each individual element and contours of equal strain potential are shown on Fig. 6b. This gives the same overall impression as the FSP data. At the end of the earthquake, the dam consisted of a soft interior core surrounded by a thick, stiff shell. Although the impressions shown on Fig. 6 are useful in estimating the overall effect of an earthquake of this intensity on elements of soil throughout the dam, it is not immediately clear whether or not the stiff outer shell would be strong enough to prevent large deformations from occurring, considering that the interior of the dam had been severely weakened by the earthquake.



|||||

(a) Factor of Specified Performance      Note: Shaded area is part. saturated, not included in analyses.



|||||

(b) Strain Potential

**FIG. 6 CALCULATED SEISMIC STABILITY, DRY DRY CANYON DAM, 2-D,  $a_{max} = 0.1g$**



## PERMANENT DEFORMATION ANALYSIS

The strain potential data shown on Fig. 6b relate only to individual samples or unconnected soil elements. The permanent deformation method described herein is based on the techniques involved in the previously described method, up to the point of assessing the significance of the stresses and strain potentials at individual elements. It is then reasoned that the permanent deformations resulting from a seismic disturbance could be calculated by an additional finite element analysis which incorporated the changes in stiffness of the soil caused by cyclic loading.

A simple model for the proposed permanent deformation method is illustrated in Fig. 7 for the case of a single element or a sample of soil. The total deformations throughout the entire life history up to and after the end of an earthquake are idealized in two separate stages: initial deformations before the earthquake  $u_i$  and the deformation during the seismic disturbance  $u_p$ .

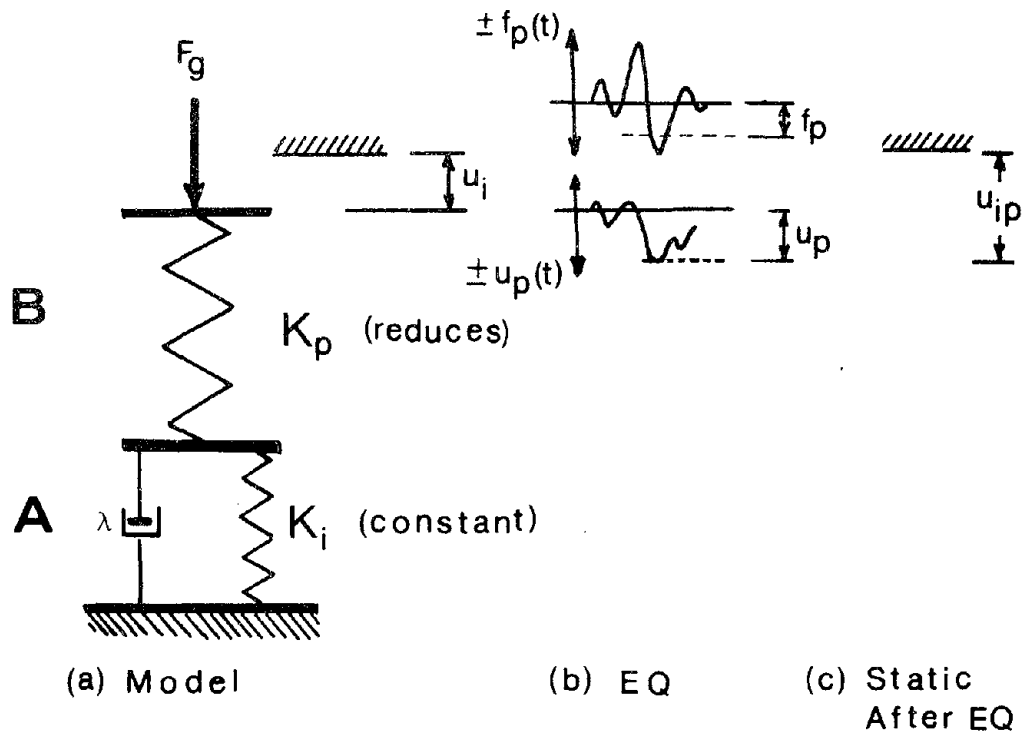


FIG. 7 ANALOGY FOR SEISMIC INDUCED PERMANENT DEFORMATIONS.

The spring and dashpot simulations shown in the model are simply figurative and used to illustrate a mechanism for separating the pre-earthquake, earthquake, and final post earthquake behavior of an element and a soil sample. The dashpot damping  $\lambda$  is high so that deformations within element A can only occur during a long period of sustained static loading. The spring stiffness  $K_i$  remains constant throughout all stages. The stiffness  $K_p$  is comparatively large before the earthquake, but as the earthquake continues  $K_p$  decreases progressively.

At any time the total stiffness of the soil is made up of two stiffnesses,

$$K_{ip} = \frac{1}{\frac{1}{K_i} + \frac{1}{K_p}} \quad (4)$$

The static, pre-earthquake gravity load on the sample or element is represented by  $F_g$ . The initial displacement corresponding to this load is  $u_i$ . Because of the relative stiffnesses of the two springs before the earthquake, for the initial gravity loading  $K_p \gg K_i$ , so that  $K_{ip} \approx K_i$ . Thus the initial displacement is made up almost entirely of compression in Element A.

The pulsating loading induced by the earthquake, or the simulation of this loading in a laboratory cyclic load test is shown by  $\pm f_p(t)$ . This is a transient pulsating force which is superimposed on the constant static gravity force  $F_g$  for a short period of time only. The corresponding deformations during this cyclic loading period are indicated by  $\pm u_p(t)$ . They are due entirely to the spring in Element B. The equivalent average cyclic force is denoted by  $f_p$ , and the maximum accumulative displacement after any elapsed time is denoted by  $U_p$ . Because  $K_p$  decreases progressively as the earthquake continues, the values of  $u_p(t)$  are not necessarily symmetric and are not constant with time. Since it is the permanent and not the cyclic deformation which is of interest in this study, the value of  $U_p$  used in the subsequent calculations is taken as the maximum accumulative displacement at the end of the earthquake, or at any other intermediate time that may be desired.

Note that in the laboratory test the sample is free to deform unrestrained whereas the corresponding element of soil in the field must deform within the limitations of the constraints of other elements and boundaries. Thus the field deformation of any particular element may be different from the value of  $u_p$  measured in a cyclic triaxial test, even though the element stiffness will have the potential to develop this displacement, if it were free of constraints.

A pseudo secant spring constant for Element B may be used to define the accumulative deformation  $u_p$  by comparing it with the causative loads. One definition for such a pseudo spring constant might be:

$$K_{p1} = \frac{F_g + f_p}{u_p} \quad (5)$$

whereas another definition might be:

$$K_{p2} = \frac{f_p}{u_p} \quad (6)$$

Either equation could be used to define  $u_p$  knowing the other terms. The numerical values of  $K_{p1}$  and  $K_{p2}$  are different because of the way in which the gravity force  $F_g$  is included. If Eq. 5 is used,  $F_g$  must be included as part of the applied force. If Eq. 6 is used, the effect of  $F_g$  is present, but unseen, since the value of  $K_{p2}$  must be obtained by cyclic testing with a constant value of  $F_g$  also applied. For the purposes of this study, the concept of Eq. 6 was used in defining a pseudo spring constant  $K_p$ , for the permanent deformation calculations.

Actually in this study, solid finite elements are used instead of simple springs. However the same analogy applies if pseudo modulus values are used to define the stiffness matrices corresponding to the single spring stiffnesses illustrated in Fig. 7. Thus a pseudo value for the initial nodal point deformations  $\underline{U_i}$  in the dam before the earthquake are defined by a linear elastic gravity-turn-on analysis with element stiffnesses formed from an appropriate static secant modulus  $E_i$ .

To define the softening during pulsating loading, a pseudo secant modulus is calculated from the results of cyclic loading laboratory tests on samples anisotropically consolidated to the appropriate field static gravity stresses.

$$E_p = \frac{\sigma_{dp}}{\epsilon_p} \quad (7)$$

Thus, for example, if the cyclic loading data in Fig. 5 corresponds to tests performed to simulate conditions at a particular element in the field, and the design earthquake is represented by  $N_{eq} = 8$  uniform cycles of stress  $\sigma_{dp} = 0.55 \text{ kg/cm}^2$ ; the corresponding accumulative axial strain in the laboratory specimen would be  $\epsilon_p = 0.7$  percent. From these data the pseudo modulus is calculated;  $E_p = 0.55/0.007 = 78 \text{ kg/cm}^2$ .

Having defined  $E_i$  and  $E_p$ , an overall secant modulus is defined by

$$E_{ip} = \frac{1}{\frac{1}{E_i} + \frac{1}{E_p}} \quad (8)$$

Using element stiffnesses defined in terms of  $E_{ip}$  along with the static gravity loads in a gravity-turn-on analysis will lead to total displacements at each nodal point  $\underline{U_{ip}}$  from the beginning of construction to the end of the earthquake. Finally by subtracting the calculated pseudo initial displacements from the total displacements, the net displacements due only to the earthquake are obtained:

$$\underline{U_p} = \underline{U_{ip}} - \underline{U_i} \quad (9)$$

Making the calculations using finite elements allows for the effect of the constraints of other elements and boundaries which are not accounted for in the previously described individual element strain potential method.

To apply this analogy to a finite element analysis of an earth dam, values of secant modulus  $E_i$  and  $E_p$  must be obtained for each element of soil. Approximate values for  $E_i$  may be estimated from static tests or from typical published values. Great accuracy is not required since the actual seismic induced permanent deformations are almost independent of the initial strains.

Values of  $E_p$  for each element must be obtained from pulsating loading tests on samples which represent the particular element in the field in terms of density, static stress and pulsating stress conditions. Details of how a data bank from a number of tests can be conveniently stored in a computer and values of  $E_p$  calculated for a

\* Underlined terms indicate a matrix quantity containing values for the entire system.

a wide variety of possible conditions is presented in Appendix I.

The assumption that the earthquake induced deformations can be represented by a sudden change in secant modulus does not necessarily imply that these deformations all occur suddenly or during the earthquake. For some soils it would be expected that some time might be required for the dam to readjust to the new modulus conditions, which might take several minutes following the earthquake. In fact, eyewitness accounts of the Hebgen dam (25) and the absence of any wave action produced by the major slide at the Lower San Fernando Dam (22) actually suggested that this was the case at these dams.

Because the permanent deformation analysis method outlined above involves only elementary modifications to any linear static finite element program, the details will not be presented here. It is important to point out however, that the stress-strain matrix is expressed in terms of bulk and shear modulus, B and G, rather than in terms of Young's modulus E and Poisson's ratio  $\nu$  as pointed out by Clough and Woodward (2), changes in the shear stiffness of a soil do not necessarily mean simultaneous changes in the volume compressibility, which would be the case if the stiffness matrix were evaluated directly in terms of E and  $\nu$ , with E changing. This objection is overcome by first evaluating B and G from the conventional relations:

$$B = \frac{E}{3(1 - 2\nu)} \quad \text{and} \quad G = \frac{E}{2(1 + \nu)} \quad (10)$$

and then evaluating the stress strain matrix  $\underline{C}$  from:

$$\underline{C} = \begin{bmatrix} (3B + 4G)/3 & (3B - 2G)/3 & 0 \\ & (3B + 4G)/3 & 0 \\ \text{(SYM)} & & G \end{bmatrix} \quad (11)$$

where  $\underline{C}$  is defined by the equation  $\underline{\sigma} = \underline{C}\underline{\epsilon}$

Values of Poisson's ratio are selected arbitrarily ( $\nu = 0.25$  to  $0.35$  for partly saturated soil and  $\nu = 0.45$  for saturated soil) and held constant for both steps. The bulk modulus B is evaluated by Eq. 10 using  $E = E_1$ . The same value of B is used in both steps. The shear modulus G is evaluated separately in each step by Eq. 10 using  $E_1$  for Step 1 and  $E_{1p}$  for Step 2. It is then used with B to calculate  $\underline{C}$ , and finally the total stiffness matrix. Thus, the effect of the seismic disturbance is to reduce the shear stiffness, without changing the volumetric compressibility of the soil.

In the pre-earthquake static stress analysis used to calculate the equilibrium consolidation stresses, the seepage forces through the dam are included with the gravity forces in evaluating the static loads. However, during the earthquake, the internal pore pressures and seepage conditions will be temporarily altered by an unknown amount. The effect of these pore pressure changes is included in the softening of the laboratory soil sample during cyclic loading. Therefore in the permanent deformation analysis, the effect of the reservoir forces were accounted for by applying an equivalent static fluid pressure along the upstream face of the dam. The internal gravity loads are calculated using total or buoyant unit weights, depending on the location of the elements with respect to the pre-earthquake phreatic line.

#### PERMANENT DEFORMATION STUDIES - DRY CANYON DAM

An example of the results obtained from this type of analysis is illustrated for the Dry Canyon Dam using the same input data as described earlier. The soil parameters for the partly saturated zones above the phreatic line were estimated from trends of increasing relative density, assuming that the partly saturated soil was somewhat stronger than soil at 100 percent relative density. The calculated permanent deformations at each nodal point are shown in Fig. 8 along with a photograph of the actual dam following the earthquake. Note that the calculated deformations are shown to an enlarged scale as compared to the base drawing. The calculations indicated that for  $a_{max} = 0.1g$ , the crest of this 63 foot high dam would settle about 2 ft and move upstream about 0.6 ft. Actual survey measurements after the earthquake indicated that the crest of the dam settled about 0.3 ft. and also moved upstream about the same amount.

At first glance, it might be concluded that there was poor agreement between the observed and calculated movements. However, as mentioned earlier, the base accelerations were not well known and the calculations were made for a peak horizontal acceleration of 0.1g, which was about midway between the probable range of 0.07g to 0.16g.

Therefore additional calculations were made to study the effect of different maximum base accelerations on the resulting permanent deformations. In each case, the calculated relative deformation pattern was similar to that shown in Fig. 8, but the actual values differed depending on the input base acceleration. The calculated crest movements for different input base accelerations are summarized in Fig. 9. For the low but plausible maximum horizontal base acceleration of 0.075g, the calculated crest displacement was only 0.78 ft. settlement and 0.15 ft. movement upstream. This compares favorably with the observed movements of 0.3 ft. in the same directions.

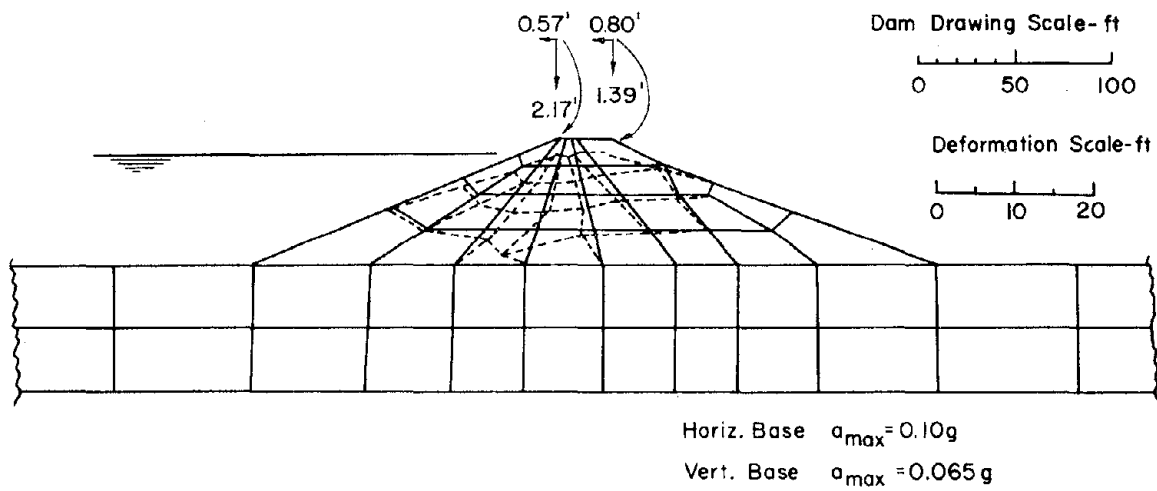


FIG. 8 PERMANENT DEFORMATION PATTERN OF DRY CANYON DAM.

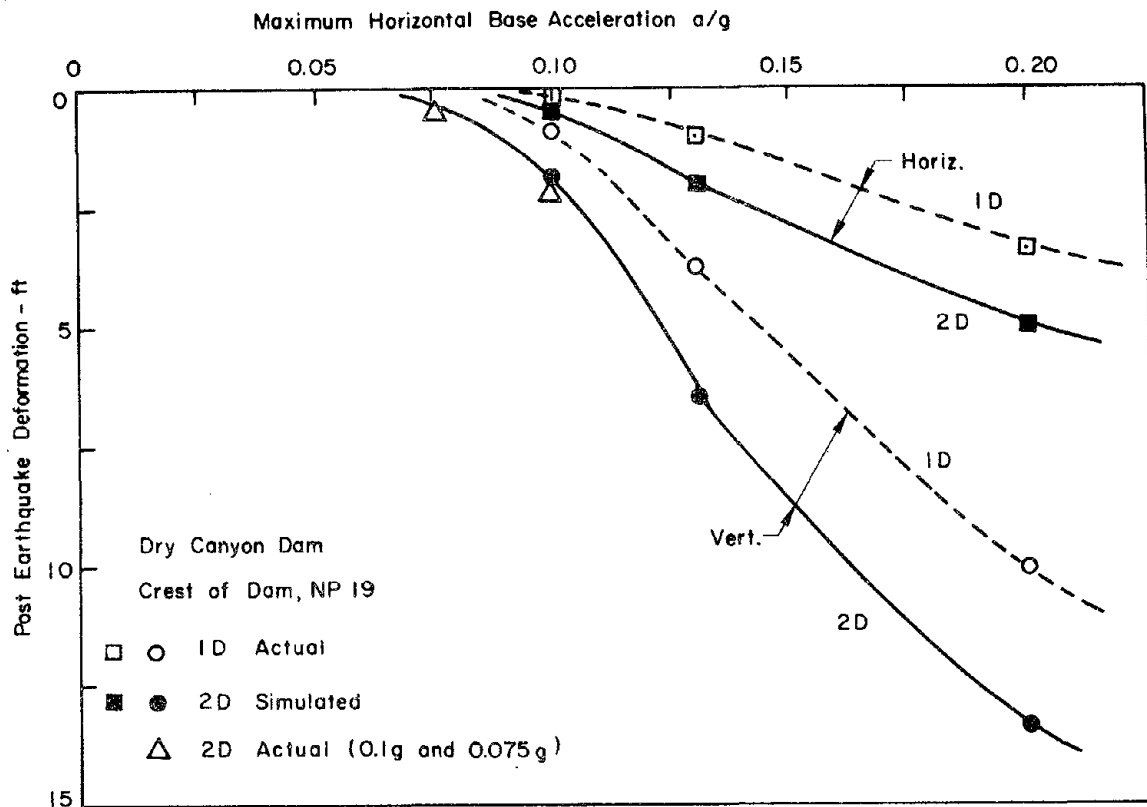


FIG. 9 COMPARISON OF CREST DISPLACEMENT FROM 1D AND 2D INPUT BASE MOTIONS.

The data in Fig. 9 also illustrates the potential vulnerability of this dam to a larger earthquake. A maximum base acceleration of 0.13g leads to a calculated crest movement of 6 ft down and 2 ft horizontal while a 0.2g base acceleration indicates a catastrophic movement of some 13 feet. (The dam has been out of service for repairs since 1966). It is seen that the maximum base acceleration is a key factor in assessing the seismic stability of earth dams.

A number of other studies were also performed for the Dry Canyon dam to investigate the relative influence of different input parameters. Space here will permit only a brief summary of the results, which are described in more detail elsewhere (10).

2-D versus 1-D seismic response analysis. The seismic response analyses referred to thus far were all performed using both horizontal and vertical based accelerations. The 1952 Taft records were used with the same multiplying factor applied to both the vertical and the horizontal accelerations. For comparison, several 1-D analysis were also performed using only the horizontal accelerogram. The maximum seismic shear stresses in various elements were found to range from 0 to 30 percent greater for the 2-D than for the 1-D cases. The overall average was about 13 percent. The computed permanent deformations at the crest for both the 2-D and the 1-D analyses are both shown on Fig. 9 where they may be directly compared.

Pre-earthquake modulus,  $E_i$ . Since the initial deformations resulting from the initial secant modulus  $E_i$ , are subtracted from the final permanent deformations (Eq. 6), it would be expected that the net results should be almost independent of  $E_i$ . Analyses were performed with three values of  $E_i$  in the ratio 0.5 : 1 : 2.0. The results indicated that any significant calculated permanent deformations from these three cases differed by less than 25 percent.

Pre-earthquake gravity stresses. To study this effect, the pre-earthquake gravity stresses were computed by three different finite element methods; a linear gravity-turn-on program, a non-linear program using hyperbolic stress-strain laws written by Kulhawy et al. (6) and a non-linear program written by the author using octahedral stress-strain relations. The maximum vertical stresses calculated by the three programs differed by about 12 percent and the maximum horizontal shear stresses differed by about 23 percent. The calculated significant permanent deformations resulting from these three sets of initial stresses differed randomly throughout the dam by about 10 to 60 percent. The largest percentage differences occurred at locations of the smallest displacements.

R-Neq reduction to equivalent uniform stress cycles. As described by Lee and Chan (8), there exists theoretically a large number of R-Neq combinations which can be used at each element to convert the actual erratic stress time history to an equivalent uniform cyclic stress comparable to the lab data. Furthermore, the same combinations should apply to all elements. Several combinations were used for parametric studies. For all reasonable values, the differences in computed permanent deformation ranged from 10 to 80 percent, the largest percentage differences being associated with the smallest deformations.

Summary of Dry Canyon studies. The parametric studies which have been performed on the Dry Canyon dam suggest that the most significant input parameter is likely to be the base acceleration. Changing the peak input acceleration from 0.075g to 0.13g (within the range predicted for this earthquake) led to a 10 fold change in calculated permanent deformation at the crest. By comparison, reasonable variations of other parameters caused less than 1 fold change in any significant calculated deformation. The problem is further complicated because of real difficulties in estimating the peak ground motions. For example, even where many records have been obtained from the same earthquake, such as at San Fernando 1971 (3), the scatter in the recorded peak accelerations at the same epicenter distance may vary by a factor of 2 or 3.

The sensitivity of the computed deformations to variations in peak acceleration and other parameters, may be slightly extreme for this dam. The interior soil was loose fine sand of the type particularly susceptible to liquefaction. Small changes in cyclic stress would tend to have a more serious effect on this dam than for well-compacted dams where cyclic loading may cause progressive strains, but not the sudden loss in strength associated with liquefaction of loose saturated sands.



## EXAMPLE ANALYSES OF OTHER DAMS

Over the years, several earth dams have been affected by earthquakes and the resulting permanent deformations reported. As a further check on the proposed method, analyses were made of four other dams, in addition to Dry Canyon. Each of these dams have been studied previously and the results reported in the literature. Space here permits only a brief description. The soil data used for these studies was either the same as used in previous analyses or, where no previous tests were performed, the parameters were estimated from the trends indicated by the available laboratory data. A brief description of each study is given below, and the significant results of the studies on all 5 dams are summarized in Table 1.

Sheffield Dam, Santa Barbara Earthquake, 1925. The failure of this 25 ft. high dam of loose silty sand has been described and analyzed by Seed et al. (20). The analyses performed herein used a higher phreatic surface than used for the previous study, but nevertheless one which was compatible with contemporary descriptions of saturation by flow around and under the upstream cutoff, and observed seepage water at the downstream toe prior to the earthquake. The same input base motion as used by Seed et al. (20) ( $a_{\max} = 0.15g$  from a modified El Centro earthquake), was also used in this study. A photograph of the actual failed dam, along with a summary of the computed deformations are shown on Fig. 10. The calculated crest movements of this 25 ft high dam were 9 ft vertical and 2 ft horizontal. The agreement appears to be satisfactory.

Upper San Fernando Dam, San Fernando Earthquake, 1971. An aerial photograph of this dam, and a sketch of the cross section showing the earthquake effects are shown in Fig. 11. The dam was located about 6 miles from the epicenter of a magnitude 6.6 earthquake, and somewhat nearer to the causitive fault. It was about 65 ft high above a 50 ft thick alluvium foundation. As a result of the earthquake, the dam cracked and the crest moved downstream about 5 ft and settled about 3 ft. Using the same input data as used by Seed et al. (22) ( $a_{\max} = 0.6g$ ), the calculated crest movements were 1 ft vertically down and 0.4 ft downstream. When the seismic stresses were increased by 20 percent, corresponding to a peak base acceleration of about 0.7g, the calculated crest movements were 1.7 down and 1.1 horizontal downstream. (The 0.7g peak acceleration corresponds to the maximum value suggested by Schnabel and Seed (14) for the epicentral zone of a magnitude 6.6 earthquake). The calculated displacements agree in direction, and in general order of magnitude, but the numerical values are somewhat smaller than the observed movements.

Lower San Fernando Dam, San Fernando Earthquake, 1971. This dam was about 130 ft high above a thin alluvial foundation. It was located within about one mile of the Upper Dam and affected by the same earthquake. An aerial view of the Lower San Fernando Dam, and the results of the permanent deformation analyses are shown on Fig. 12. As seen in the photograph, a major slide developed in the upstream face, with observed movements of about 40 ft down and 20 ft upstream. Using the same input data as Seed et al. (22) ( $a_{\max} = 0.56g$ ), the calculated crest movements were only 5 ft vertically down and 2.5 ft upstream. If the seismic stresses were

TABLE 1  
SUMMARY OF PERMANENT DEFORMATION OBSERVATIONS AND CALCULATIONS

Dam	Type	Height ft.	Earthquake	Mag.	Horiz. $a_{max}$ (g)	Crest Deformation - ft. Observed (Calculated)		Remarks	Ref.
						Vertical	Horizontal		
Dry Canyon	Hydraulic fill and rolled silty sand	63	Taft 1952	7.7	0.075	0.3 D (0.8 D)	0.3 US (0.15 US)	2 inch crack. $a_{max}$ is lower limit of range	7
Sheffield	Loose silty sand	25	Santa Barbara 1925	6.3	0.15	Failed (8.7 D)	Failed (1.9 US)	Dam failed and reservoir emptied. Assumed lower 12 ft saturated.	20
Upper San Fernando	Hydraulic fill silty sand	65	San Fernando 1971	6.6	0.6 0.7	3.0 D (1.0 D) (1.7 D)	5.0 DS (0.4 DS) (1.1 DS)	Major crack on US slope. Pressure ridge DS toe. $a_{max}$ from Ref. 22. Seismic stresses 20% greater than for $a_{max} = 0.6$	22
Lower San Fernando	Hydraulic fill silty sand	130	San Fernando 1971	6.6	0.56 0.67	40 D (5 D) (12 D)	20 US (2.5 US) (5.5 US)	Major slide upstream. $a_{max}$ from Ref. 22. Seismic stresses 20% greater than for $a_{max} = 0.56$	22
Hebgen Sta. 5+00	Loose soil and rock fill	87	Montana 1971	7.6	0.4	2.8 D (2.1 D)	0.8 DS (0.7 US)	Crest settled by core wall. $a_{max}$ middle of range.	23, 24, 25

D = vertically down  
DS = horizontally downstream  
US = horizontally upstream

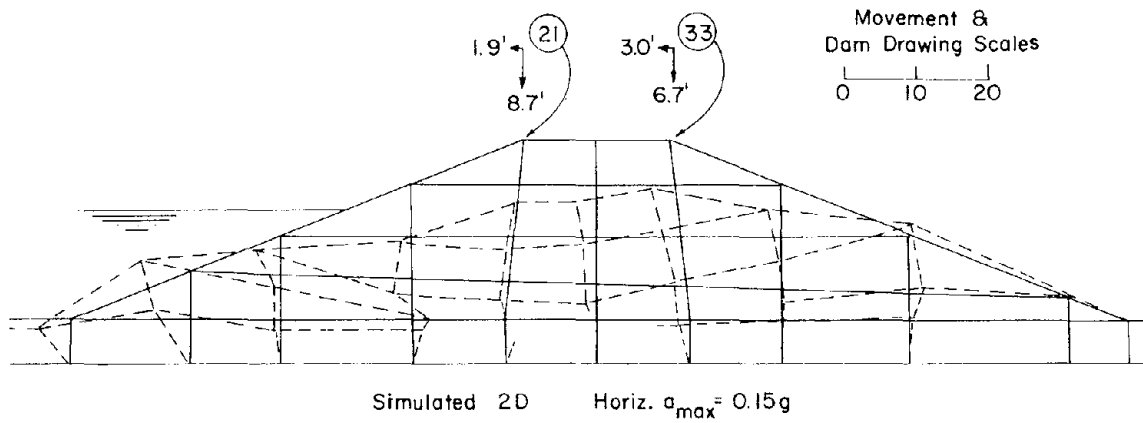
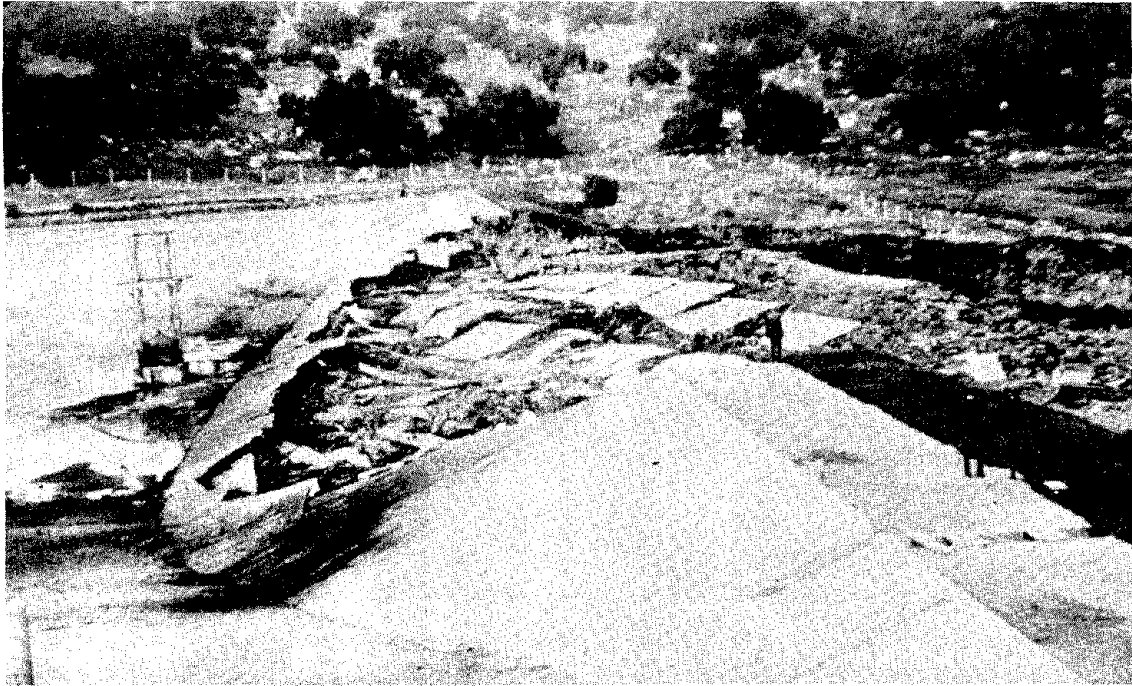
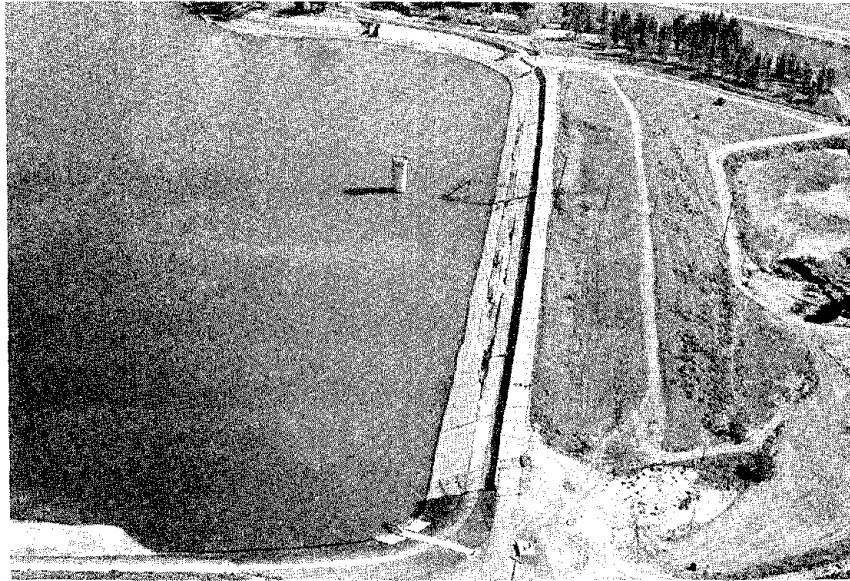
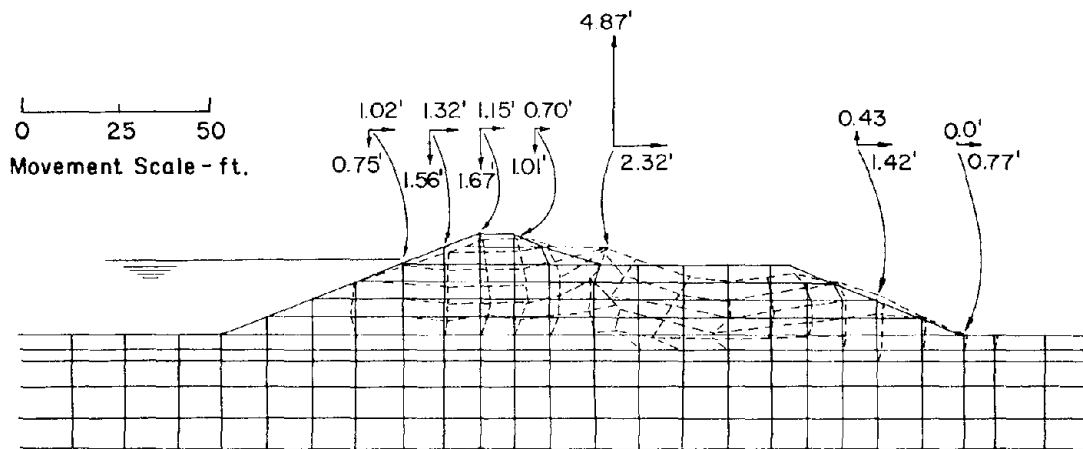
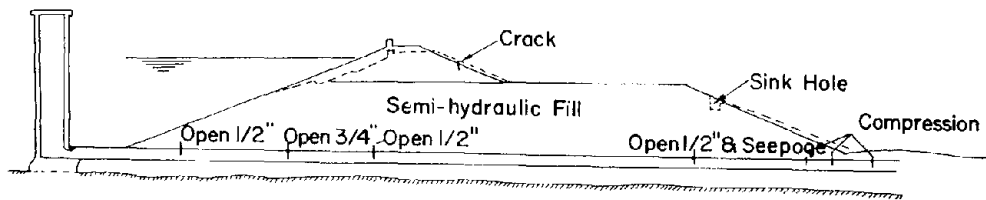


FIG. 10 PERMANENT DEFORMATION PATTERN OF SHEFFIELD DAM



0 50 100  
Scale - ft



Simulated 2D, Horiz.  $a_{max} = 0.7g$

FIG. II PERMANENT DEFORMATION PATTERN, UPPER SAN FERNANDO DAM.

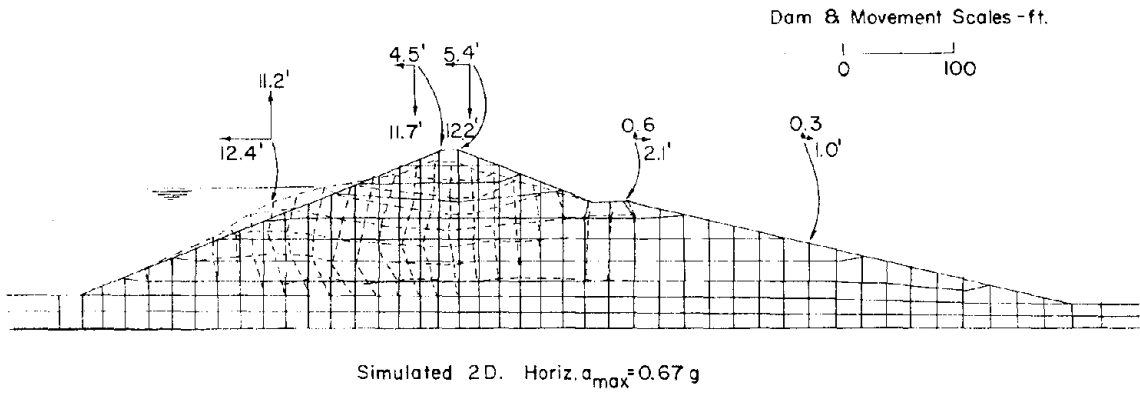
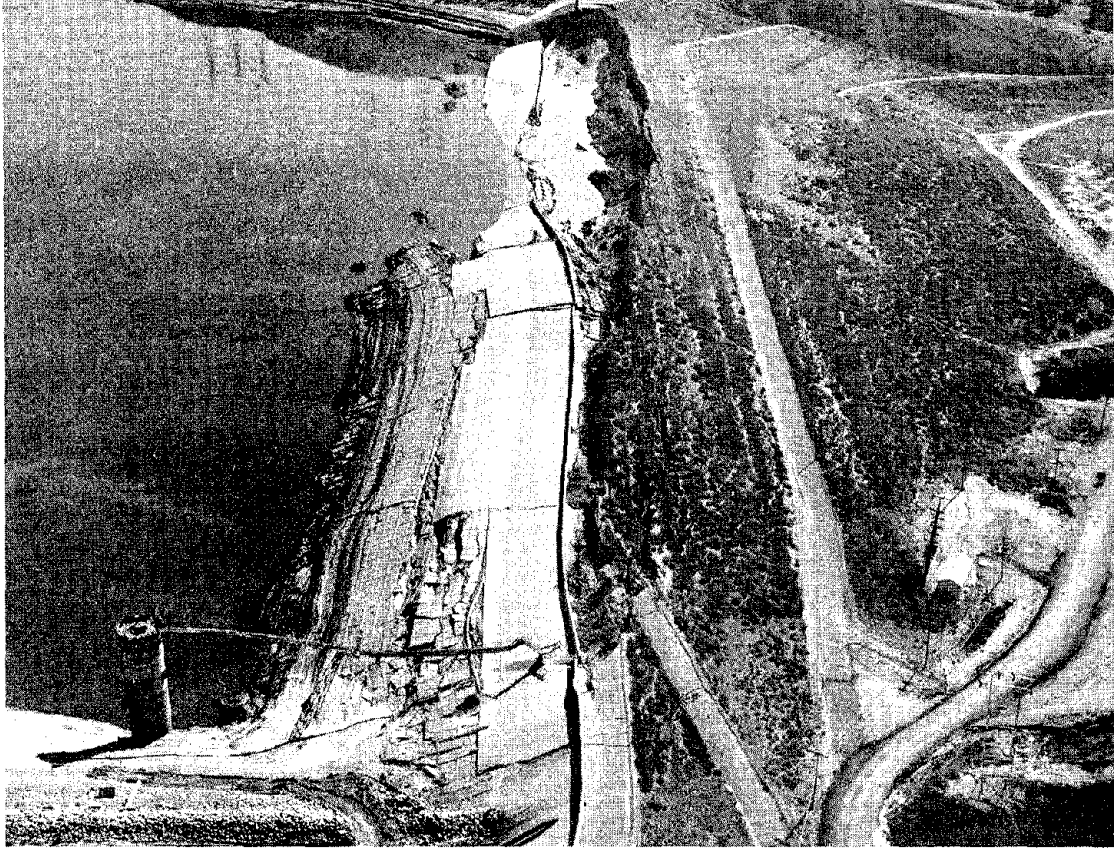


FIG.12 PERMANENT DEFORMATION PATTERN LOWER SAN FERNANDO DAM.

increased by 20 percent, corresponding to a peak base acceleration of about 0.67g, the calculated movements would increase to 12 ft down and 5 ft upstream. As with the Upper dam, the calculated movements agreed in direction and general magnitude, but were somewhat smaller than actually observed.

Hebgen Dam, Montana Earthquake, 1959. The behavior of this dam during the 1959 earthquake has been described qualitatively by several investigators (23,24,25), but a rigorous analysis has not previously been made. A photograph of the crest of the dam following the earthquake is shown on Fig. 13. Of interest is the 6 ft vertical fault scarp, seen horizontally across the photograph just behind the dam.

The dam was an old, earth and rockfill structure built in 1909-1914. The soil properties were estimated to be similar to the average of available data assuming relative densities in the upstream, downstream and loose rockfill sections of 55, 65 and 75 percent respectively. This is similar to the densities obtained in other dams of that vintage. The Magnitude 7.7 earthquake was estimated to have caused 0.4 g maximum horizontal acceleration at the dam site. The Taft horizontal and vertical accelerograms were used for the seismic response analysis, after modification for this maximum acceleration.

The results of the calculated and measured surface deformations are also shown on Fig. 13 and indicate good agreement.

Conclusions. A summary of the significant data on the 5 dams studied is shown in Table 1. Examination of the comparison between observed and predicted permanent deformations indicates reasonable agreement for each dam. For all but the small horizontal movement at the crest of the Hebgen dam, the direction of the calculated movements agreed with the direction of the observed movements. However in general, the calculations seemed to under estimate the actual movements. This was especially true for large observed movements which were accompanied by shearing, cracking or breaking of the outer shell such as at the San Fernando Dams.

It is recalled that the finite element method is based on small strain theory, and on assumed continuity. The best which can be expected is for the method to indicate relatively large permanent deformations, which if they did develop, could lead to further deterioration in the dam by causing an outer stiff shell to shear, crack or break. Thus, for example, at the Lower San Fernando dam, the calculated crest movements ranged from 5 to 12 feet, depending on which of the two base input accelerations were used. For these large movements to occur over the period of a few minutes, especially with the interior of the dam softened appreciably by liquefaction, one could expect further cracking and sliding to develop, which in fact did happen.

The input base motion was shown to be much more important than any of the other parameters in determining magnitudes of permanent deformation. Since the exact nature of the base accelerations is likely to be the most difficult parameter to predict in advance for any actual design, these results suggest that while improvements in the analytical and laboratory techniques are needed, these may not be as important as refinements in methods of predicting input base motions.

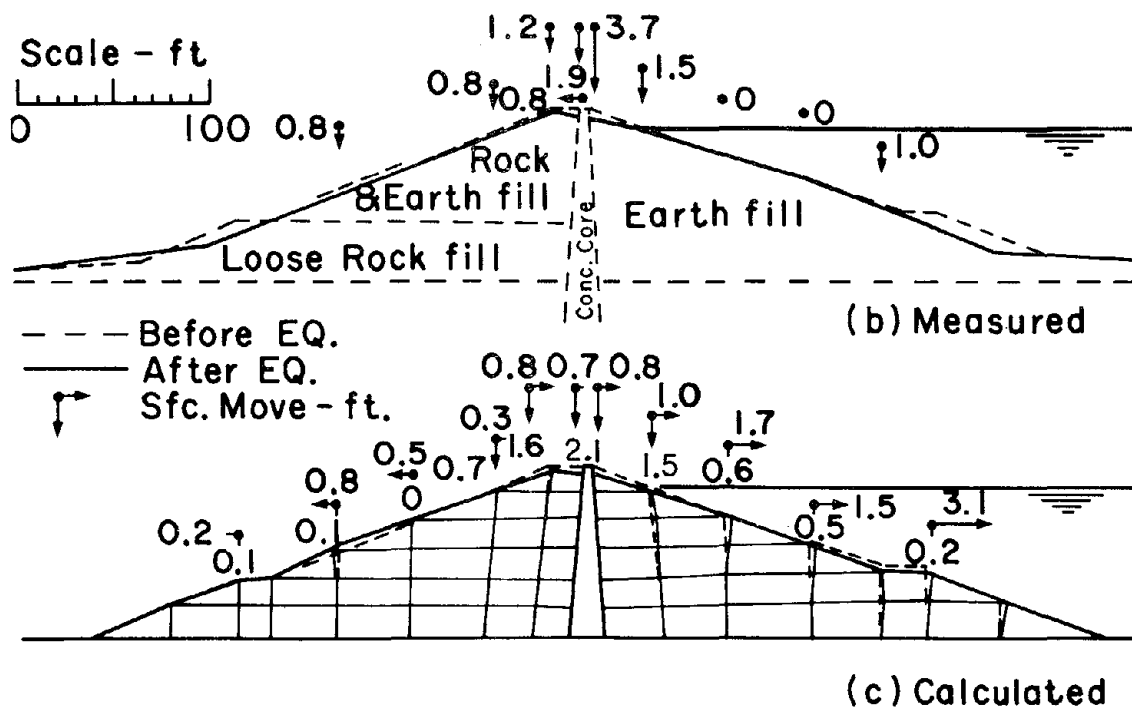


FIG. 13 PERMANENT DEFORMATIONS, HEBGEN, DAM,  
STA 5 + 00, 1959

Although much work remains to be done on the problem of predicting seismic induced permanent deformations of embankments, nevertheless, the reasonable agreement between observed and calculated movements for the cases studied tend to support the general proposed method, and it is felt that it will be useful as a possible alternative or a supplement to the existing methods for seismic stability analyses of earth dams.

#### ACKNOWLEDGEMENTS

The computer program QUAD4, used to determine the seismic stresses, was developed and supplied by the Geotechnical Engineering group, University of California, Berkeley. Data on the Hebgen Dam was furnished by the Montana Power Company. The photographs of the San Fernando Dams, Figs. 11 and 12 were by the California Department of Water Resources. The photograph of the Hebgen Dam, Fig. 13 was by K. V. Steinbrugge. The studies were performed under the auspices of a grant from the National Science Foundation. Grateful appreciation is expressed for this assistance.

#### REFERENCES

1. Ambraseys, N. N., "On the Seismic Behavior of Earth Dams", Proceedings 2nd World Conference on Earthquake Engineering, Tokyo, Japan, Vol. II, 1961, pp. 1345-1363.
2. Clough, R. W. and Woodward, R. J., "Analysis of Embankment Stresses and Deformations", Journal of the Soil Mechanics and Foundations Division, ASCE, Vol. 93 No. SM-4, July 1967, pp. 529-549.
3. Duke, C. M., et al., "Effects of Site Classification and Distance on Instrumental Indices in the San Fernando Earthquake", Report No. UCLA-ENG-7247, June 1972.
4. Goodman, R. E. and Seed, H. Bolton, "Earthquake Induced Displacements in Sand Embankments", Journal of the Soil Mechanics and Foundations Division, ASCE, Vol. 92, SM-2, March 1966, pp. 125-146.
5. Idriss, I. M., Lysmer, J., Hwang, R., and Seed, H. B., "QUAD-4 A Computer Program for Evaluating the Seismic Response of Soil Structures by Variable Damping Finite Elements Procedures", Report No. EERC 73-16, College of Engineering, University of California, Berkeley, July 1973.
6. Kulhawy, F. H., Duncan, J. M. and Seed, H. B., "Finite Element Analysis of Stresses and Movements in Embankments During Construction", Geotechnical Engineering Report TE69-4, Department of Civil Engineering, University of California, Berkeley, 1969.
7. Lee, Kenneth L. and Walters, Henry G., "Earthquake Induced Cracking of Dry Canyon Dam", paper presented at the ASCE National Meeting, October 1972, Houston, Texas, preprint no. 1794, summarized in Proceedings 5th World Conference on Earthquake Engineering, Rome, 1973, paper no. 192.



8. Lee, K. L. and Chan, K., "Numbers of Equivalent Significant Cycles in Strong Motion Earthquakes", Proceedings Microzonation Conference, Seattle, Vol. II, 1972, pp. 609-627.
9. Lee, Kenneth L. and Walters, Henry G., "Earthquake Induced Cracking of Dry Canyon Dam", Proceedings 5th World Conference on Earthquake Engineering, Rome, Italy, 1973.
10. Lee, Kenneth L., "Earthquake Induced Permanent Deformations of Dams", Report by UCLA School of Engineering and Applied Science, 1974.
11. Matthews, Samuel W., "The Night the Mountains Moved", National Geographic, March 1960, pp. 329-359.
12. Newmark, N. M., "Effects of Earthquakes on Dams and Embankments", Geotechnique, Vol. 15, No. 2, June 1965, pp. 139-173.
13. Oddi, M. M. and Humphreys, J. D., "Correspondence on Slope Stability During Earthquakes", Geotechnique, Vol. 11, No. 4, December 1961, pp. 354-356.
14. Schnabel, P. B. and Seed, H. B., "Accelerations in Rock for Earthquakes in the Western United States", Report No. EERC-72-2, University of California, Berkeley, July 1972.
15. Seed, H. Bolton, "A Method of Earthquake Resistant Design of Earth Dams", Journal of the Soil Mechanics and Foundations Division, ASCE, Vol. 92, No. SM-1, January 1966, pp. 13-41.
16. Seed, H. Bolton and Goodman, R. E., "Displacements of Slopes in Cohesionless Materials During Earthquakes", Journal of the Soil Mechanics and Foundations Division, ASCE, Vol. 92, No. SM-2, March 1966, pp. 125-146.
17. Seed, H. Bolton and Martin, Geoffrey, R., "The Seismic Coefficient in Earth Dam Design", Journal of the Soil Mechanics and Foundations Division, ASCE, Vol. 92, No. SM-3, May 1966, pp. 25-58.
18. Seed, H. Bolton, "Earthquake Resistant Design of Earth Dams", Canadian Geotechnical Journal, Vol. 4, No. 1, 1967, pp. 1-27.
19. Seed, H. Bolton and Lee, Kenneth L., "Pore Water Pressures in Earth Slopes Under Seismic Loading Conditions", Proceedings 4th World Conference on Earthquake Engineering, Santiago, Chile, January 1969.
20. Seed, H. Bolton, Lee, K. L., and Idriss I., M., "An Analysis of the Sheffield Dam Failure", Journal of the Soil Mechanics and Foundations Division, ASCE, Vol. 95, No. SM-6, November 1969, pp. 1453-1490.
21. Seed, H. Bolton and Peacock, W. H., "Test Procedures for Measuring Soil Liquefaction Under Cyclic Loading", Journal of the Soil Mechanics and Foundations Division, ASCE, Vol. 97, No. SM-8, August 1971, pp. 1099-1119.

22. Seed, H. B., Lee, K. L., Idriss, I. M., and Makdisi, F., "A Study of the Performance of the Two San Fernando Dams During the February 9, 1971 San Fernando Earthquake", Report to be published by the Earthquake Engineering Research Center, 1973.
23. Seed, H. Bolton, "Stability of Earth and Rockfill Dams During Earthquakes", Embankment Dam Engineering, Casagrande Volume, Edited by Hirschfeld and Paulos, Wiley 1973, pp. 239-269.
24. Sherard, J. L., et al., "Earth and Earth Rock Dams", Wiley 1963, pp. 164-170.
25. Steinbrugge, K. V. and Cloud, W. K., "Epicentral Intensities and Damage in the Hebgen Lake, Montana, Earthquake of August 17, 1959", Bulletin of the Seismological Society of America, Vol. 52, No. 2, pp. 181-234, April 1962.
26. Taylor, D. W., "Fundamentals of Soil Mechanics", Wiley 1948, pp. 452-453.
27. Terzaghi, Karl, "Mechanism of Landslides", Applications of Geology to Engineering Practice, (Berkey Volume), Geological Society of America, 1950, p.89.

#### APPENDIX I - PERMANENT DEFORMATION PARAMETERS FROM CYCLIC LOAD TRIAXIAL TESTS

The results of a typical set of cyclic loading, triaxial tests on samples of saturated soil are shown in Figs. 4 and 5. An actual seismic stability analysis would require several such sets of data to be obtained from laboratory tests covering the ranges of consolidation pressure density and soil type found in various zones of the dam. Since it is not practical to perform a set of tests for the conditions at every location, data from a reasonable number of tests must be stored in the computer and used as a basis for interpreting to the actual conditions at each element in the dam. This appendix describes a method for storing and using the data. The method is illustrated in detail for Dry Canyon Dam soil, but has also been found to apply equally well to other soils studied.

As a first step, the laboratory cyclic stress-strain (\*) data of Fig. 5a is plotted on log-log paper as shown in Fig. 14a where it is seen that for any axial strain  $\epsilon_1$ , the data form a straight line

$$\sigma_{dp} = C_1 \left( \frac{N}{10} \right)^{S_1} \quad (12)$$

The intercept  $C_1$  is conveniently taken at  $N = 10$  cycles because this approximates many earthquake conditions. Most soils studied thus far appear to have a unique value of slope  $S_1$ , independent of consolidation stress or axial strain. Thus  $S_1$  is the first key parameter.

(\*) Cyclic strains are defined as follows: For  $K_C = 1.0$ ,  $\epsilon_1 = \frac{1}{2}$  peak to peak strain amplitude; For  $K_C = 1.0$   $\epsilon_1 =$  compressive strain amplitude.

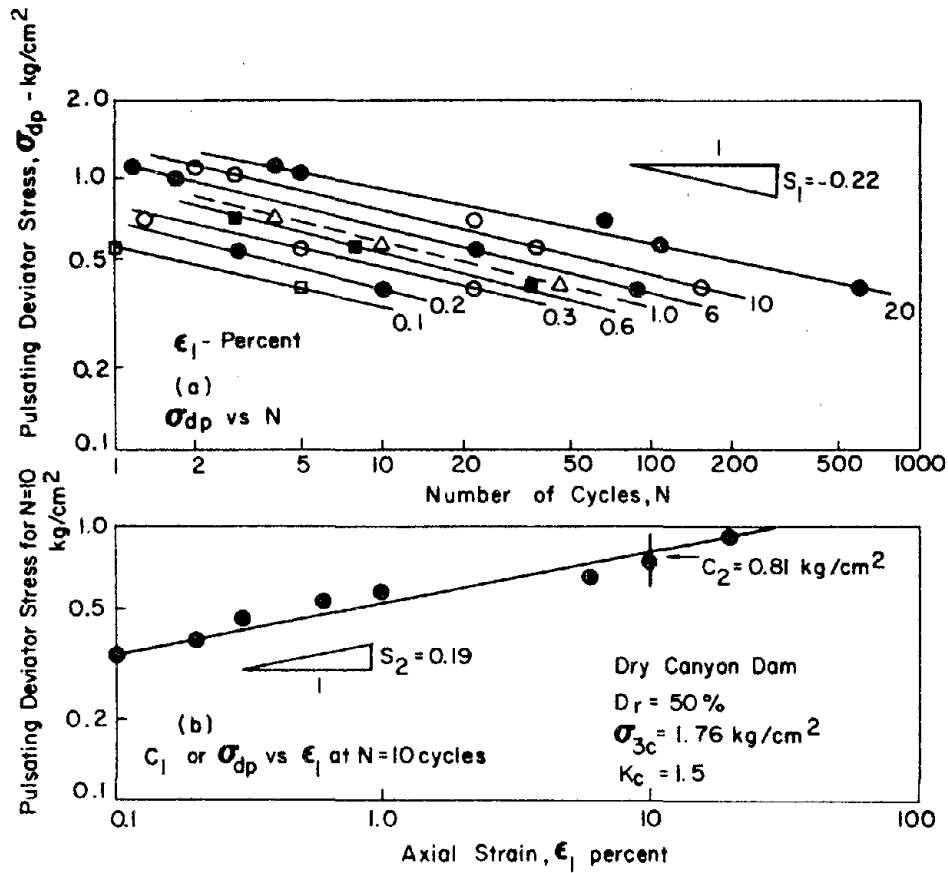


FIG. 14-PULSATING LOAD TEST RESULTS TO LOG-LOG SCALE

Plotting  $C_1$  vs.  $\epsilon_1$  on log-log paper as shown in Fig. 14b leads to a straight line

$$C_1 = C_2 \left( \frac{\epsilon_1}{10} \right)^{S_2} \quad (13)$$

where  $C_2$  is the intercept which defines the pulsating deviator stress required to cause 10 percent axial strain in 10 cycles. The variation of  $C_2$  with  $\sigma_{3c}$  and  $K_c$  is shown in Fig. 15 to be defined by the linear relation;

$$C_2 = C_3 + S_3 \sigma_{3c} \quad (14)$$

The parameters  $C_3$  and  $S_3$  and  $S_2$  have been found to be linear functions of  $K_c$  as shown in Fig. 16, according to the equations:

$$C_3 = C_4 + S_4 (K_c - 1) \quad (15)$$

$$S_3 = C_5 + S_5 (K_c - 1) \quad (16)$$

$$S_2 = C_6 + S_6 (K_c - 1) \quad (17)$$

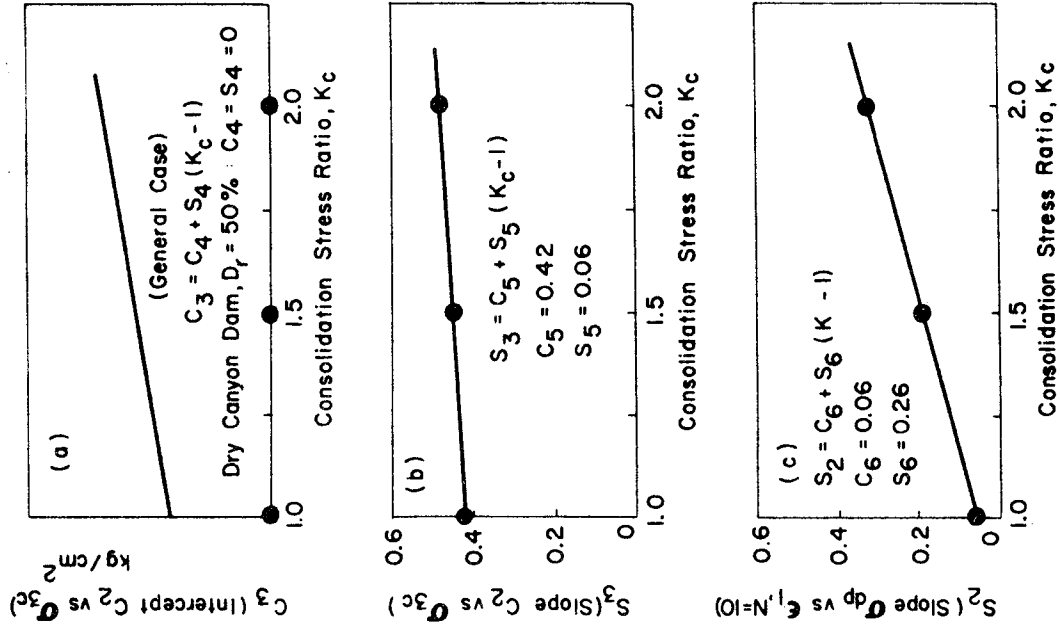


FIG. 16-PERMANENT DEFORMATION PARAMETERS AS A FUNCTION OF  $K_c$

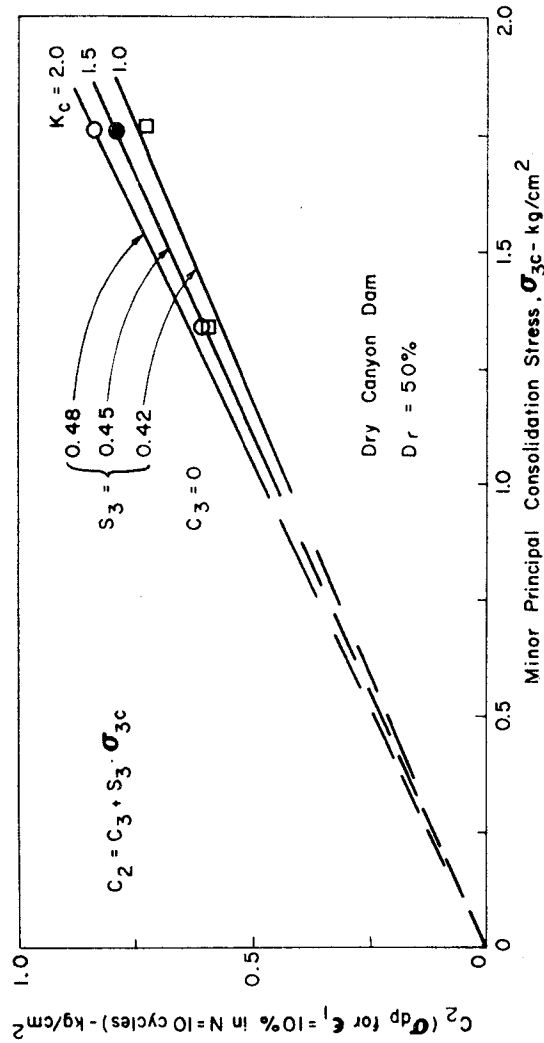


FIG. 15-PULSATING DEVIATOR STRESS TO CAUSE 10 PERCENT STRAIN IN 10 CYCLES

Thus the permanent deformation laboratory data for all anisotropic consolidation stress conditions for one soil and one density can be defined by 7 empirical parameters as used in Eqs. 12 through 17;  $S_1$ ,  $C_4$ ,  $S_4$ ,  $C_5$ ,  $S_5$ ,  $C_6$ ,  $S_6$ . Numerical values for these 7 parameters are readily obtained from a minimum of about 9 cyclic loading triaxial tests for each major zone of soil in the embankment. (3 values of  $\sigma_{3c}$  and 3 values of  $K_c = 1.0, 1.5,$  and  $2.0$ ). After some rearrangement of the foregoing equations, the following expression is obtained for the axial strain in a laboratory sample subjected to  $N$  cycles of uniform stress intensity  $\pm \sigma_{dp}$ .

$$\epsilon_1 = 10 \left( \frac{N}{10} \right)^{-\frac{S_1}{S_2}} \left( \frac{\sigma_{dp}}{C_2} \right)^{\frac{1}{S_2}} \quad (18)$$

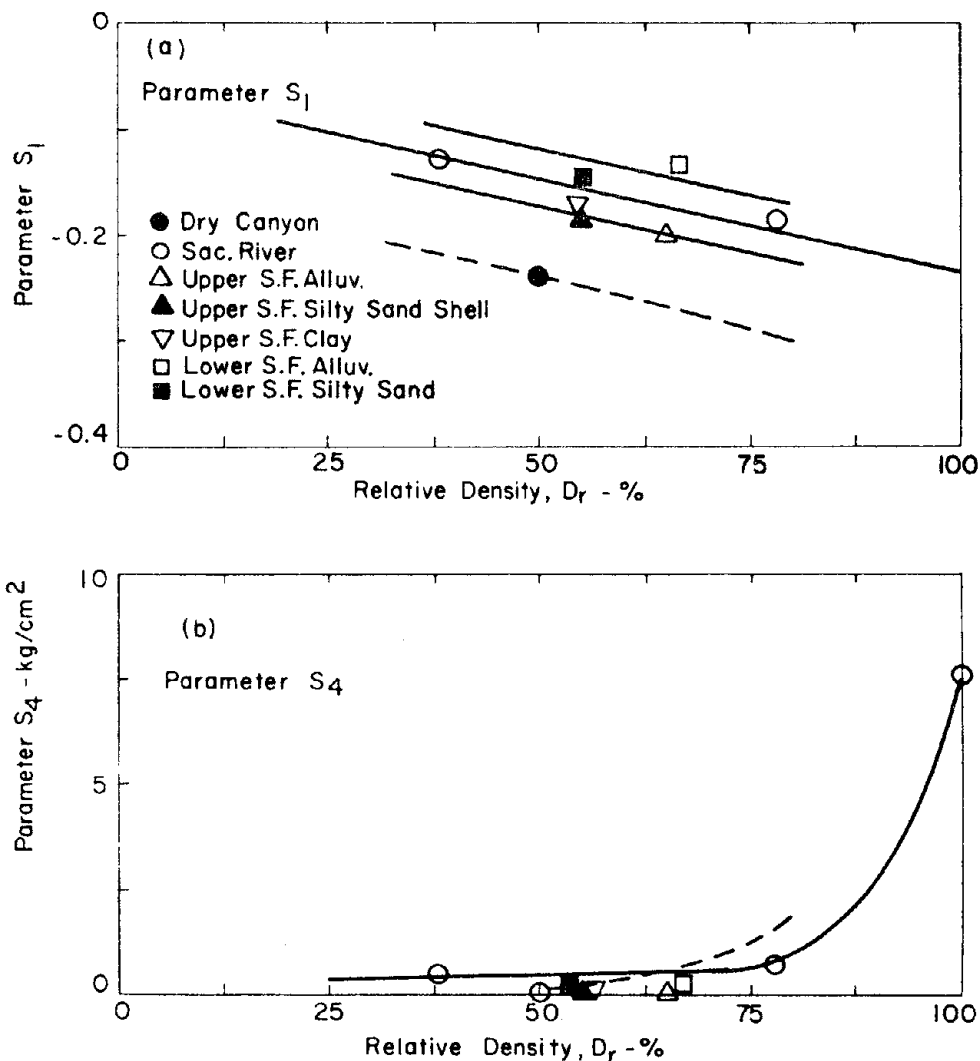


FIG. 17-COMPILATION OF PERMANENT STRAIN PARAMETERS FROM VARIOUS SOILS (1 OF 4)

For an actual problem, values for  $N$  and  $\sigma_{dp}$  at each element are obtained from the pulsating shear stress  $\tau_p$  and  $N_{eq}$  calculated by a seismic response analysis to a given earthquake and applying Eq. 1 in reverse. The axial strain  $\epsilon_1$  is identical to the strain  $\epsilon_p$  used in the main text. The secant modulus  $E_p$ , is defined by Eq. 7 using  $\epsilon_p$  from Eq. 15 and  $\sigma_{dp}$  from the seismic response analysis.

The 7 key parameters have been evaluated from available data on 7 different soils at several relative densities. A comparative compilation of these data are shown in Figs. 17 through 20. The data show a fairly consistent pattern which may be a useful reference for comparison with data from other soils, as they become available. Data for the Upper San Fernando Dam hydraulic fill clay was plotted at  $D_r = 55\%$  because that was the relative density of the hydraulic fill silty sand at the same dam.

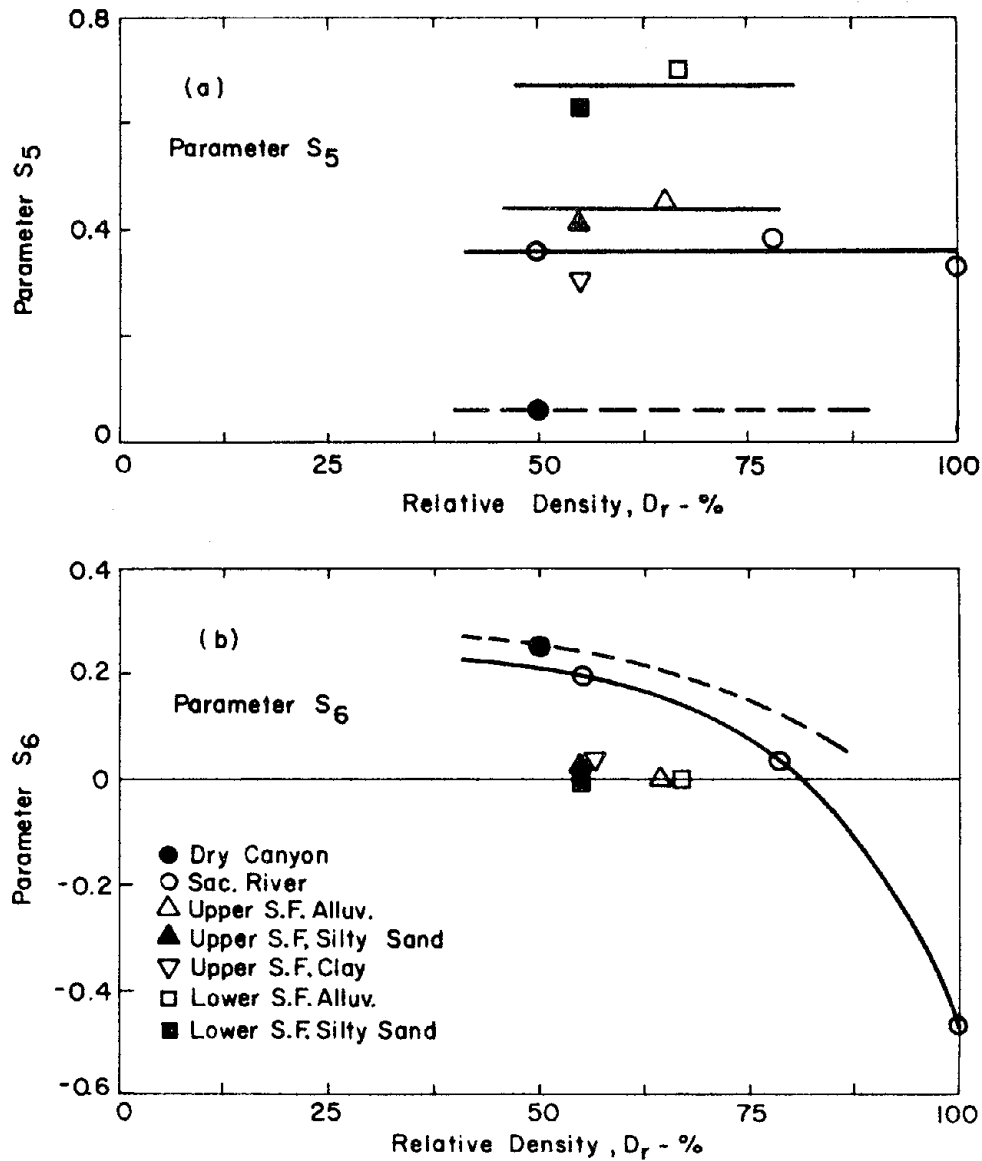


FIG. 18-COMPILATION OF PERMANENT STRAIN PARAMETERS FOR VARIOUS SOILS (2 of 4)

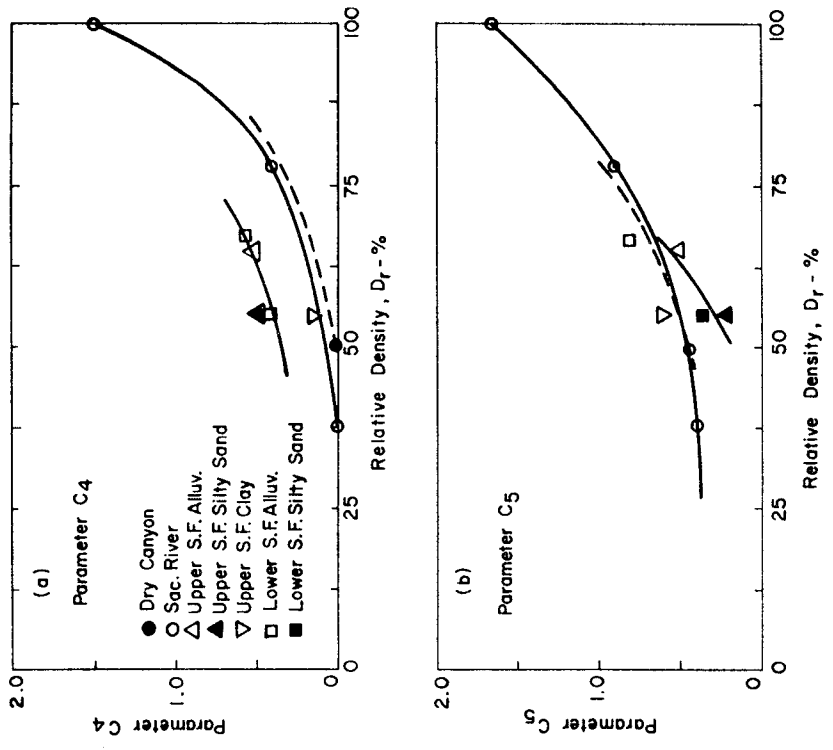


FIG. 19-COMPILATION OF PERMANENT STRAIN PARAMETERS FOR VARIOUS SOILS (3 of 4)

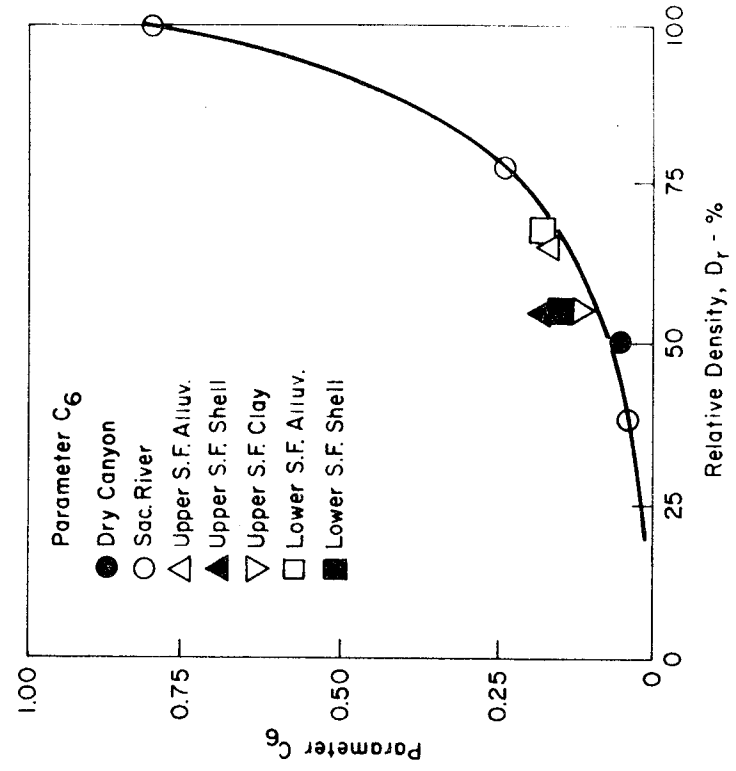


FIG. 20-COMPILATION OF PERMANENT STRAIN PARAMETERS FOR VARIOUS SOILS (4 of 4)